Research on complex hydrodynamic interaction when UUV recovered by submarine

***LUO Yang, †PAN Guang, Yang Zhi-dong, HUANG Qiao-gao, and QIN Deng-hui**

College of Marine, Northwestern Polytechnical University, Xi'an, China

*Presenting author: lawyer0818@hotmail.com

†Corresponding author: panguang601@163.com

Abstract

Hydrodynamic interaction performance between an unmanned underwater vehicle (UUV) and a submarine was presented using Reynolds Average Navier-Stokes (RANS) techniques, when submarine was recovering an UUV. The hydrodynamic characteristics of UUV in different positions relative to submarine was simulated numerically based on RANS techniques, and the variation of UUV's hydrodynamic coefficients interfered by flow around the submarine was analyzed. Then combined with the dynamic grid techniques, unsteady hydrodynamic performance was numerically calculated when an UUV performed parallel movement and vertical movement relative to the longitudinal axis of the submarine, and the changing law of the hydrodynamic coefficients of UUV under corresponding conditions was revealed. The method presented could predict the maneuvering and controlling performance of the UUV retrieved to a submarine.

Keywords: Computational Fluid Dynamics, Hydrodynamic Interaction, Unmanned Underwater Vehicle, Submarine.

Introduction

With the exploitation of marine resources being intensified and more extensive military applications, the Unmanned Underwater Vehicle (UUV) is required to have longer operation time. For an UUV equipped in a submarine, energy refuel and information exchange can be achieved through underwater recovery[1]. Ronald W. Yeung and Wei-Yuan Hwang[2] has predicted nearfield hydrodynamic interactions of ships in shallow water based on the slender-body theory. H. Zhang[3] et al. studied effect of turbulence intensity to the fluid dynamic interference of two cylinders side in side. Zeng Yifei[4] presented equivalent extension-body method to calculate the interaction between two underwater cylinders in relative motion. Y.R. Choi[5] investigated the hydrodynamic interference between floating multi-body system with the boundary element method. Wang Fei[6] developed a program based on the panel method and calculated the hydrodynamic performance of an underwater vehicle in motion near the submarine. B.J. Koo[7] and S.Y. Hong[8] simulated numerically the hydrodynamic interaction and mechanical coupling effects of two floating platforms and vessels connected by elastic lines respectively. Chen Li and Zhang Liang et al.

pointed that the minimal interaction path exists for underwater bodies in approaching process in theory from the computation results of a cylinder near a plane wall according to potential flow theory[9], and according to the combination bodies in periodic heave and pitch motion in unbounded flow field and near a plane wall, they used unsteady theory method to calculated nonlinear unsteady interference force related to the vortex evolution and motion. They, based on which, also revealed the typical characteristics of unsteady hydrodynamic interference. The hydrodynamic characteristics of a 2D oval with length-thickness ratio 7.0 while moving near plane wall were presented through towing-tank tests by them, then, they gave the regressive formula of hydrodynamic coefficients relative to clearances, attack angles and divided three typical interaction regions, defined as Lifting, Mixed and Blocking Region[10]-[11]. HeYuzhi[12] simulated the process that an UUV approached a conical docking device with numeral method and obtained the change law of drag coefficient and lift coefficient of the UUV during which. Leong, Z. [13] investigated the hydrodynamics performance when an AUV moved in various horizontal and vertical positions of a submarine at a series of relative speeds with CFD method based on N-S equation. S.A.T. Randeni P.[14] et al. investigated the hydrodynamic interaction between an AUV operating in close proximity to a submarine, with the development of a CFD model to replicate the pure sway motion of the AUV and figured out that the percentage difference between the CFD and EFD (experimental fluid dynamics) sway forces were generally below 6%.

However, UUV's appendages were not taken into consideration in most of the researches above. Steady and unsteady hydrodynamic performance between an UUV and a submarine was numerically calculated based on RANS techniques and the results of UUV models with appendages were compared with which without attached parts in this paper. The condition in focus is more complex and more applicable to engineering reality, which may provide a reference for prediction and analysis on the hydrodynamic performance during UUV's underwater recovery.

1 Calculated Models

1.1 Geometric models and calculated conditions

An axisymmetric body with characteristic diameter D = 0.534m and length L = 7m was elected as UUV model and the model without appendages was defined as UUV-1 while the other one with which was identified as UUV-2. The distance from the buoyancy center of the UUV-1 to the head is 3.2446m while which of the UUV-2 is 3.2499m. As for submarine model, the research utilized a 1:18 scaled model of the SUBOFF submarine hullform as the submarine's main body and defined as SUB-1, while the model with complete appendages including the main body, fairwater and caudal fin as UUV-2. The full length L_s of the submarine model is 78.408m, length between perpendiculars L_{pp} is 76.698m and maximum diameter D_s of which equals 9.144m. In addition, dimensionless fluid force and torque coefficients are defined as

$$C_{xx} = f_{xx} / \left(\frac{1}{2} \rho S_a U^2 \right), \quad M_{xx} = m_{xx} / \left(\frac{1}{2} \rho S_a U^2 \right) \qquad (1)$$

In the formula (1), f_{xx} and m_{xx} represent the component of fluid force and torque along the direction of the coordinate system *xx* respectively, while C_{xx} and M_{xx} correspond to the dimensionless coefficient of fluid force and torque components. The largest cross-sectional area of the UUV model was selected as S_a and UUV's full length was considered as L_a in dimensionless hydrodynamic coefficients. The L_a and S_a of submarine's dimensionless hydrodynamic coefficients were set as L_{pp} and its square accordingly.

In order to facilitate the description of working conditions and the analysis of calculation results, a coordinate system *oxyz* was established and the feature positions of UUV relative to the submarine were defined as shown in Figure 1.

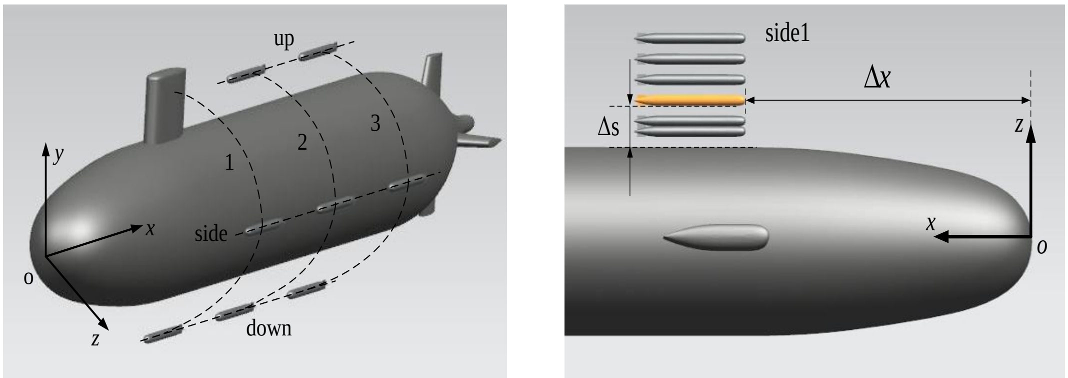

(a) 3D **(b) *xoz***

Figure 1 The coordinate system definition and feature positions of UUV relative to the submarine

As shown in Figure 1 (a), the central point of the bow was defined as the coordinate origin, the *ox* axis is along the vertical symmetry axis of the submarine, *oy* axis lies in submarine's longitudinal symmetry plane and vertical to the *ox* axis, and the *oz* axis meets the right-hand rule. The position of the UUV relative to the submarine was determined by its longitudinal position(the coordinate of the UUV along the *ox* axis) and relative direction, and chose three different longitudinal positions along the *ox* axis relative to the submarine and labeled as "1, 2, 3" respectively. When the UUV model situates in the submarine's lateral plane, it is recorded as "side"; in the submarine's vertical plane and the positive *ox* axis, it is denoted as "up", otherwise as “down”. Based on the definition of the above markers, the feature orientation of the UUV relative to the submarine can be represented as “side1” and “down2”. As depicted in Figure 1 (b), take “side1” as the example, the distance from the UUV’s wall to the submarine’s was marked as Δs. Therefore, the feature position of the UUV relative to the submarine can be obtained with the combination of feature orientation and Δs, which was denoted as “side1-Δs”. The *ox* coordinate of the UUV’s head point was marked as Δx. In order to study the influence of UUV’s three different longitudinal position: near the head, tail and central of the submarine, on the hydrodynamic coefficients, the values of Δs corresponding to three different longitudinal position labeled as “1, 2, 3,” are shown in Table 1.

Table 1 The values of Δs corresponding to different longitudinal position

ox axis label	1	2	3
Distance Δx (m)	18	31.5	45

1.2 Meshing

A rectangular domain with a size of $5L_s \times 20D_s \times 20D_s$ was chosen as computational domain. The SUBOFF model was arranged in the center of the domain, and the distance from the velocity inlet to the head of the model is $1.5L_s$. Except for the velocity inlet and pressure outlet, the four remaining faces of the rectangular domain were set as slip wall.

Structured grid was utilized for computational domain meshing, and based on based on the concept of block partition, the computational domain of a single submarine was generated firstly, then a portion of grid blocks in the overall calculation domain was excised and embeded in the grid block containing the UUV model inside the overall domain through internal interface to complete the grid generation, which is as shown in Figure 2 and Figure 3.

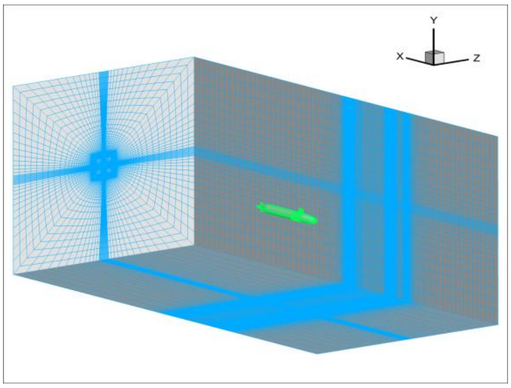

Figure 2 The overall grid generation

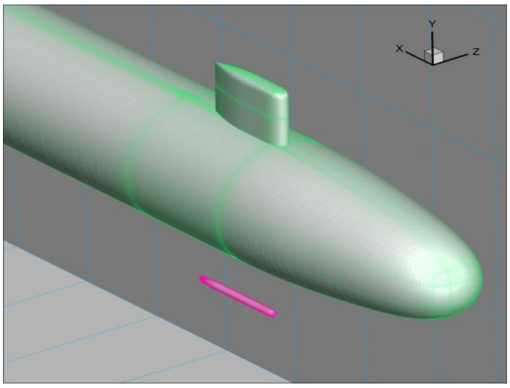

Figure 3 The merged grid generation

For the unsteady motion, used dynamic layering method to simulate the motion of the interface of the UUV and whole grid in the dynamic area relative the submarine.

2 Analysis of steady hydrodynamic interference between the UUV and submarine

2.1 Results and analysis of hydrodynamic interference of models without appendages

The turbulence model selected was RNG k - ε and set inlet velocity as 2 kn ignoring the influence of gravity.

Figure 4 to Figure 6 shows the pressure coefficient distribution corresponding to three feature orientations: “side1”, “side2” and “side3” when Δs = 0.5. From the pressure coefficient contours in the lateral *xoz* section it can be seen that: in “side1” feature orientation the head of the UUV-1 model was close to the low pressure area of the SUB-1 head, and influenced by which the pressure drag of the UUV-1 got smaller than that in unbounded flow condition, even resulted in a pressure surplus (a negative value). Therefore, the hydrodynamic interference of the flow around the submarine to the UUV-1 performed as drag reduction. In “side2” feature orientation, the tail of the UUV-1 model was close to the low pressure area of the SUB-1 aft body and influenced by which the pressure drag of the UUV-1 got bigger than that in unbounded flow condition, so the hydrodynamic interference increased the resistance. While in “side2” feature orientation, the UUV-1 was in the stable flow field near the parallel middle part of the SUB-1, and the low pressure area near the SUB-1 tail had little effect on the UUV-1, as a result, the pressure drag of the UUV-1 approximated that in unbounded flow condition. It can be seen from pressure coefficient contours in the local transverse *yoz* section that the isobar shaped as an inverted “C” type, namely a low pressure region formed in the adjacent zone of the UUV-1 and SUB-1, which shows that the SUB-1 acted suction on the UUV-1.

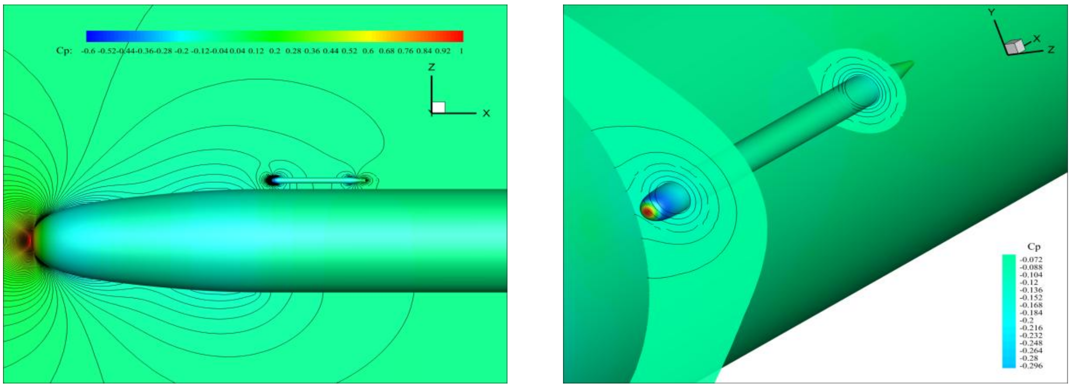

（a）**The lateral *xoz* section** （b）**The local transverse *yoz* section**

Figure 4 The pressure coefficient distribution in the position “side1-0.5m”

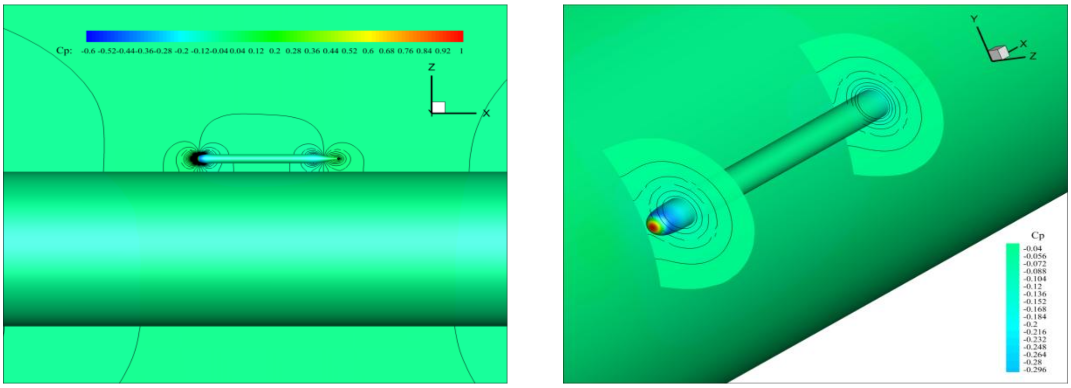

（a）The lateral *xoz* section　　　（b）The local transverse *yoz* section

Figure 5 The pressure coefficient distribution in the position “side2-0.5m”

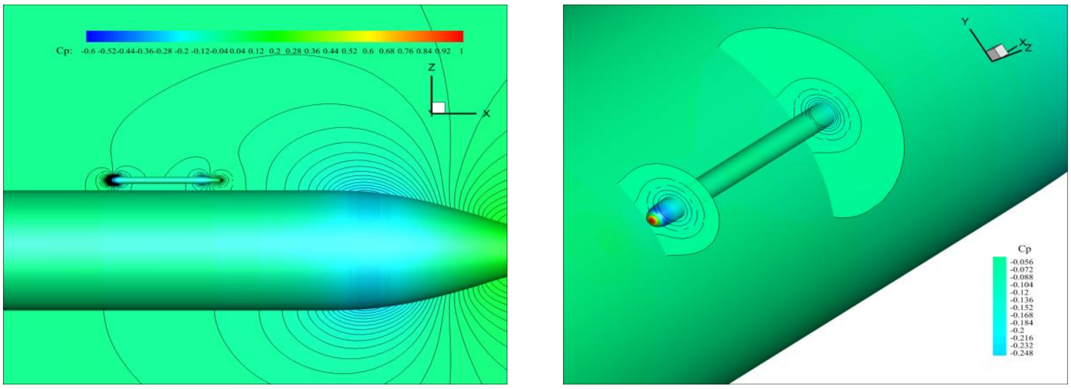

（a）The lateral *xoz* section　　　（b）The local transverse *yoz* section

Figure 6 The pressure coefficient distribution in the position “side3-0.5m”

Now defined the dimensionless distance from the UUV’s wall to the submarine’s as $\Delta\overline{s}$ and the UUV’s diameter was selected as the feature space. The variation of the drag coefficient C_x with $\Delta\overline{s}$ according to the three feature positions of the UUV-1 above was as shown in Figure 7. Regarded the drag coefficient of the UUV-1 in unbounded flow field as reference value, Figure 8 shows the change percentage of the resistance coefficient with $\Delta\overline{s}$.

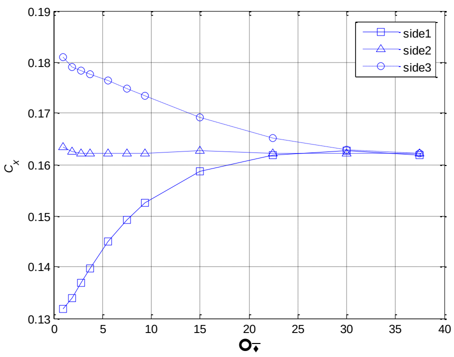

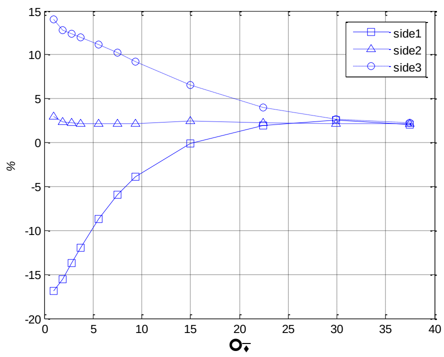

Figure 7 C_x corresponding to $\Delta\overline{s}$　　**Figure 8 The change percentage of C_x**

According to Figure 7 and Figure 8 it can be found that when the UUV-1 was located in “side1” near the head of the submarine, C_x of the UUV-1 decreased with the decrease of $\Delta\bar{s}$; while in “side2” where the flow field was stable, C_x varied little; however, C_x increased with the decrease of $\Delta\bar{s}$ in “side3”. And C_x approached to the value in unbounded flow field with the increase of $\Delta\bar{s}$ under the three conditions. When $\Delta\bar{s}$ >30, C_x of the UUV-1 corresponding to the three conditions all tended to converge, in another word, the interference function distance of the flow around the SUB-1 on UUV-1 model is about 30 times its diameter.

2.2 Results and analysis of hydrodynamic interference of models with appendages

The turbulence model selected was also RNG k - ε and set inlet velocity as 2 kn ignoring the influence of gravity as well as the condition without appendages.

The model with full appendages involved eight different feature orientations. For the convenience to analyze the hydrodynamic interference of the flow field in different feature orientations, defined the plane determined by the longitudinal axes of the SUB-2 and SUB-2 as the main interference plane, based on which, the main interference force coefficient along the vertical direction to the *ox* axis was marked as C_{xx}, and suction was recorded as positive, repulsion as negative; the main interference moment coefficient vertical to the main plane was denoted as M_{xx}, the moment deviating the head of the model UUV-2 from the SUB-2 was denoted by positive, otherwise negative.

The numerical results of C_x and its change percentage compared to the unbounded condition corresponding to different feature orientations are shown in Figure 9.

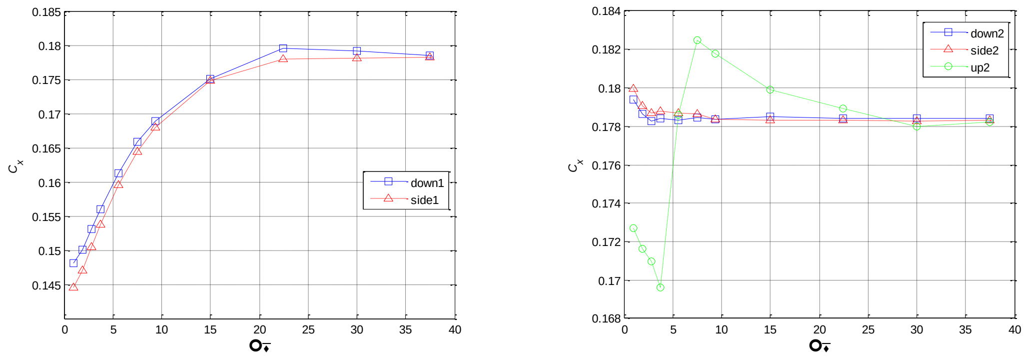

(a) Result in longitudinal position “1 （b）Result in longitudinal position “2”

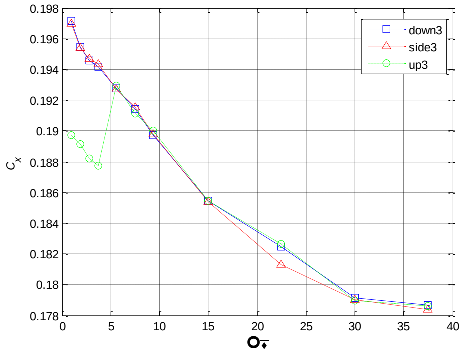

（c）Result in longitudinal position “3”

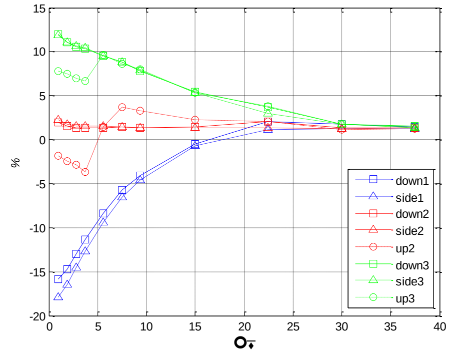

（d）The change percentage of C_x

Figure 9 Results of C_x and its change percentage compared to that in unbounded condition

It can be seen from Figure 9 that when the UUV was in the same longitudinal position and the relative direction was “side” and “up”, the change laws of C_x with $\Delta\bar{s}$ were almost identical. For the condition “up2”: when $\Delta\bar{s} \leq 4$, frictional resistance was small, pressure drag was large and the overall was small for the flow field around fairwater; when $\Delta\bar{s} > 5.6$, with the increase of $\Delta\bar{s}$, the model UUV-2 got close to the up edge of the wake flow and the interaction on frictional resistance decreased while the interference to frictional resistance came to an effect gradually; when $\Delta\bar{s} = 7.5$, C_x in the condition “up2” was larger than that in the conditions “side2-4m” and “down2-4m”; when $\Delta\bar{s} > 7.5$, the wake flow of the fairwater had little effect on the velocity field of UUV-2, with the increase of $\Delta\bar{s}$, the influence of local high pressure in the wake flow of the fairwater on the UUV-2 weakened and C_x decreased; when $\Delta\bar{s} = 22.5$, C_x approximated that in “side2” and “down2”. For the condition “up3”: the interaction of the wake flow of the fairwater on C_x mainly concentrated the range of $\Delta\bar{s} \leq 4$, when $\Delta\bar{s} > 5.6$, C_x approximated that in “side3” and “down3”. From Figure (d), the interference distance of the flow around the SUB-2 on UUV-2 model is about 30 times its diameter.

The calculated results of C_{xx} and M_{xx} of the UUV-2 in different longitudinal positions are as shown in Figure 10 to Figure 12. Graphical results show that when the UUV was in the same longitudinal position, and the relative directions were “side” and “up”, the change laws of C_{xx} and M_{xx} with $\Delta\bar{s}$ were almost consistent, C_{xx}

both performed as suction; when $\Delta\bar{s}$ =5.6 and $\Delta\bar{s}$ =7.5, for the collective influence of the wake flow of the fairwater and submarine's external flow, C_{xx} corresponding to "up2" was negative, performed as repulsion; C_{xx} corresponding to "up3" was a small positive value close to zero, performed as slight suction; when $\Delta\bar{s}$ ≥9.4, the change laws of C_{xx} and M_{xx} with $\Delta\bar{s}$ in position "up" were almost consistent with the conditions in "side" and "down". When the longitudinal position was "1", M_{xx} were all positive, so the moment deviated the head of the UUV-2 from the SUB-2, and with the increase of $\Delta\bar{s}$, it increased firstly and then decreased, similar to parabola change rules; as the longitudinal position was "2", with the increase of $\Delta\bar{s}$, the change trends of M_{xx} in "side" and "down" conditions were almost identical and they both decreased at first and then remained stable approximately, but due to the influence of the wake flow of the fairwater , when $\Delta\bar{s} < 9.4$, the curve of M_{xx} in "up" condition is similar to an inverted "N" type, then M_{xx} tended to be stable as well; when the longitudinal position was "3", the change of M_{xx} was consistent with the condition in longitudinal position "2".

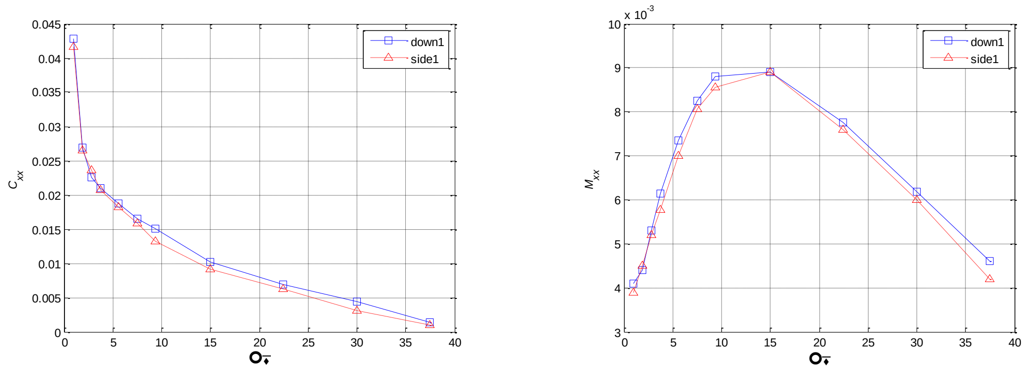

(a) C_{xx} (b) M_{xx}

Figure 10 C_{xx} and M_{xx} in longitudinal position "1"

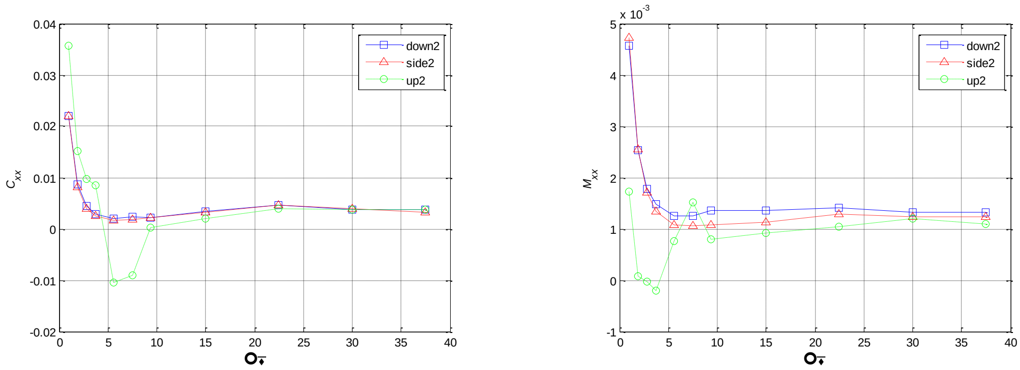

（a） C_{xx} （b） M_{xx}

Figure 11 C_{xx} **and** M_{xx} **in longitudinal position “2”**

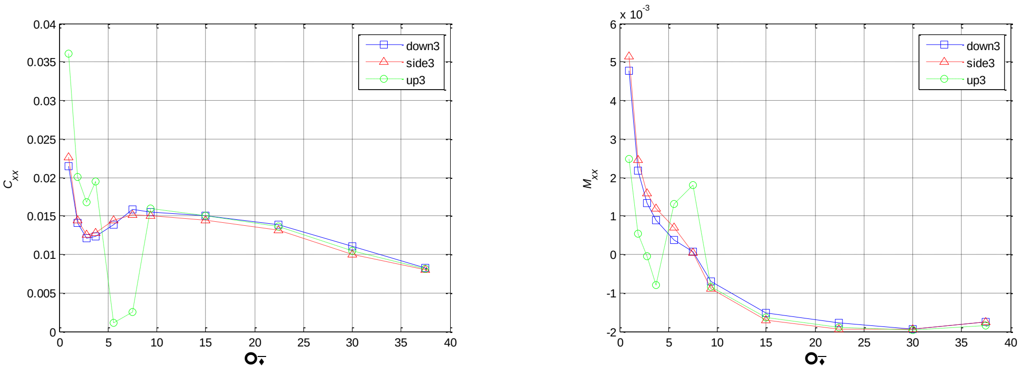

（a） C_{xx} （b） M_{xx}

Figure 12 C_{xx} **and** M_{xx} **in longitudinal position “3”**

2.3 Comparison of computational results of models with and without appendages

Selected the calculated results of the model without appendages UUV-1 and the model with appendages UUV-2 in “side” position for comparision. Figure 13 shows C_x of the model UUV-1 and UUV-2 corresponding to $\Delta\overline{s}$ in three different “side” conditions. It can be seen from the comparative results that: while in the same feature orientation, for the UUV-1 and UUV-2, the change rules of C_x with $\Delta\overline{s}$ were similar to each other and the difference between C_x of the two models corresponding to the same $\Delta\overline{s}$ basically maintained at a certain range. Combined with Figure (d), the difference was close to that in the unbounded flow field, from which we can see the hydrodynamic interference of the submarine to the UUV mainly acts on its main body and has little effect on the fin.

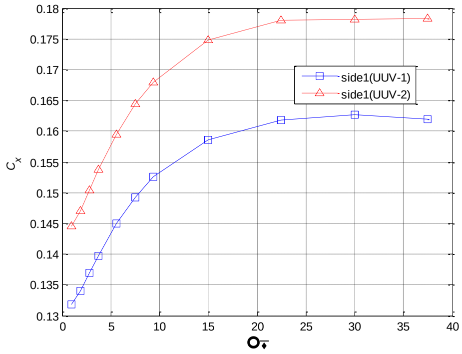

（a）“side1”

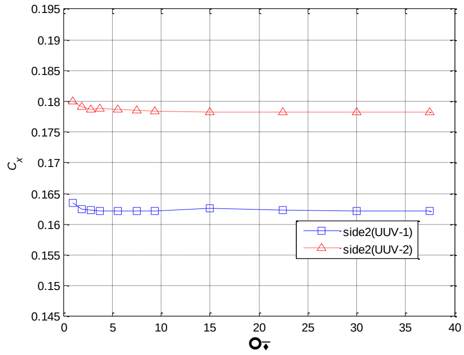

（b）“side2”

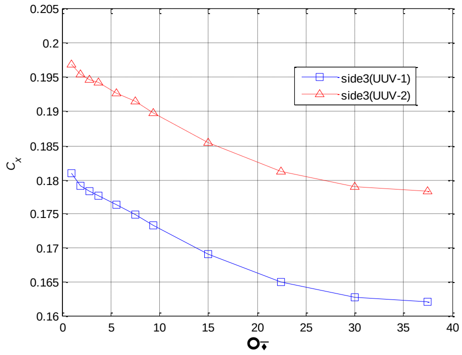

（c）“side3

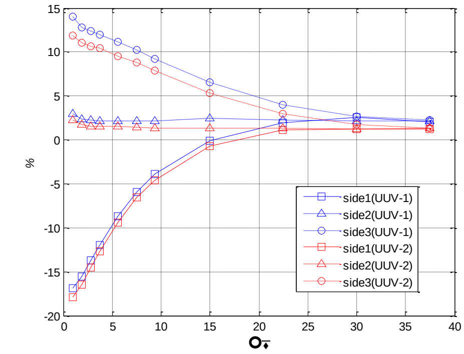

（d）The change percentage of C_x

Figure 13 C_x and its change percentage of the UUV-1 and UUV-2 in three “side” conditions

Figure 14 to Figure 16 show the side force coefficient C_z and yawing moment coefficient M_y of the model UUV-1 and UUV-2 corresponding to $\Delta\bar{s}$ in three different “side” conditions. From the comparative results we can find that in the same calculated condition, for the UUV-1 and UUV-2, the change rules of C_z and M_y with $\Delta\bar{s}$ were similar to each other. On the whole, the absolute value of C_z of the UUV-2 was bigger than that of the UUV-1, which illustrates that the side interference to the UUV was greater because of the appendages. For the condition “side1”, M_y of the UUV-2 was smaller than that of the UUV-1 corresponding to the same $\Delta\bar{s}$; for the condition “side2”, when $\Delta\bar{s}$ <2, M_y of the UUV-2 was larger than that of the UUV-1, while $\Delta\bar{s}$ >2, M_y of the two models were almost the same corresponding to the same $\Delta\bar{s}$; for the condition “side3”, when $\Delta\bar{s}$ <3.7, the absolute value of M_y of the UUV-2 was bigger than that of the UUV-1, while $\Delta\bar{s}$ >3.7, the absolute value of M_y of the UUV-2 was smaller than that of the UUV-1.

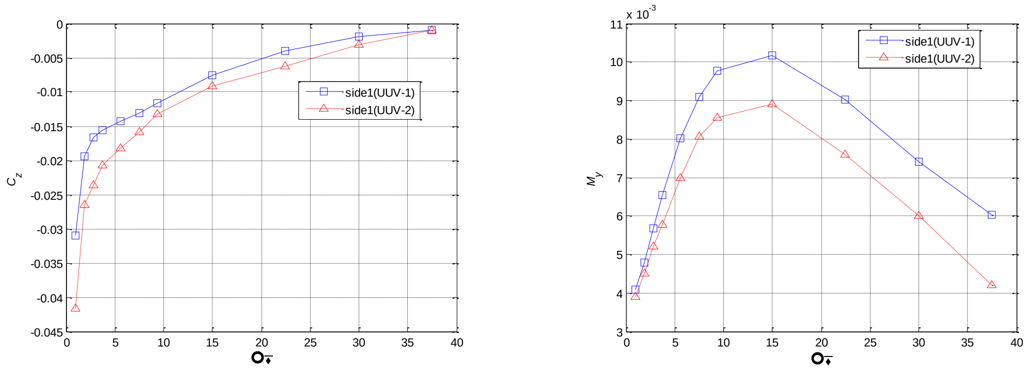

（a） C_z （b） M_y

Figure 14 C_z and M_y of the UUV-1 and UUV-2 in the condition “side1”

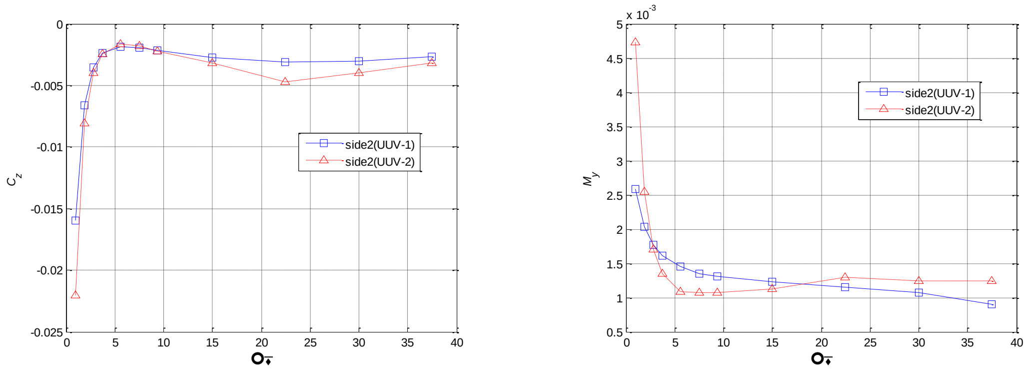

（a） C_z （b） M_y

Figure 15 C_z and M_y of the UUV-1 and UUV-2 in the condition “side2”

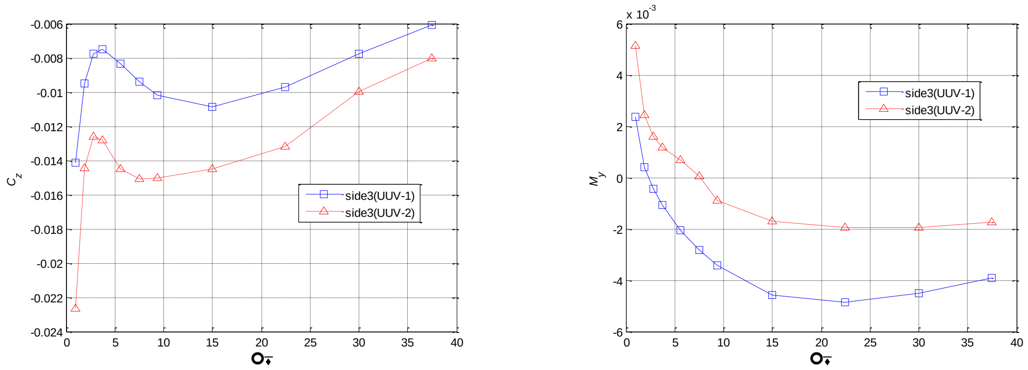

(a) C_z (b) M_y

Figure 16 C_z and M_y of the UUV-1 and UUV-2 in the condition "side3"

3 Analysis of unsteady hydrodynamic interference between the UUV and submarine

3.1 Simulation research on the motion of the UUV parallel to the submarine's longitudinal axis

Selected the light body UUV-1 and SUB-1 as the research objects and the simulation time step was 0.2s. Considering the condition that Δs =3m, the UUV-1 moved from the initial position side3-3 to side3-2 paralleled to the submarine's longitudinal axis at three different speeds 0.4kn, 0.75kn and 1kn, the change rules of the hydrodynamic coefficients of the UUV-1 with $\bar{x}$ were investigated. The specific calculation results are shown in Figure 17 to Figure 20.

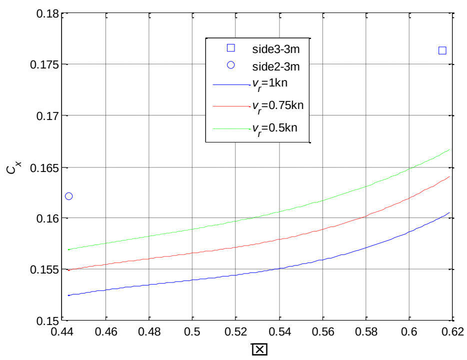

Figure 17 C_x corresponding to $\bar{x}$

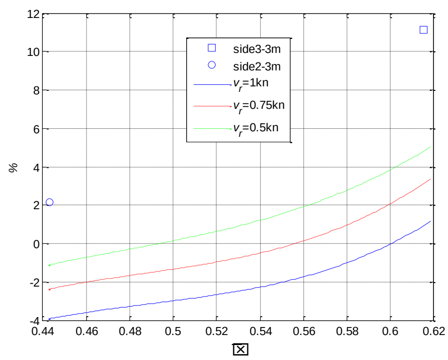

Figure 18 The change percentage of C_x

Figure 17 and Figure 18 show C_x and its change percentage while the UUV-1 moving paralleled to the submarine's longitudinal axis at various speeds. From which we can figure out that the change laws of C_x with $\bar{x}$ were similar at different rates and ΔC_x between two conditions corresponding to different speeds was about a certain value. The larger the relative velocity was, the smaller C_x was corresponding to the same $\bar{x}$, that is, resistance of the UUV was smaller.

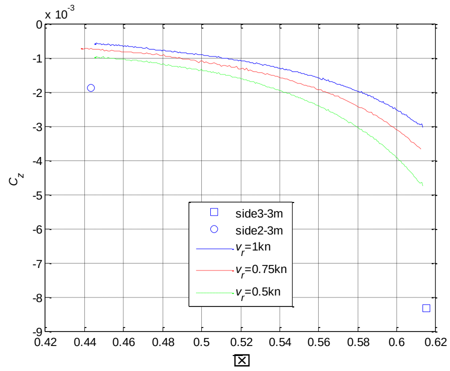

Figure 19 Calculated results of C_z

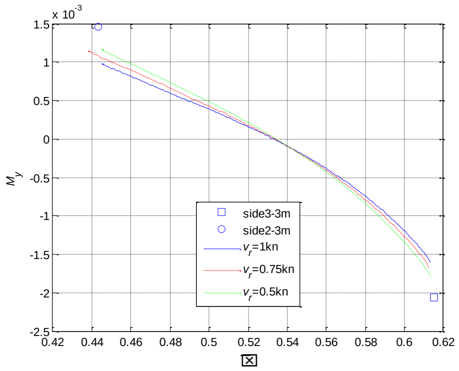

Figure 20 Calculated results of M_y

The change of C_z and M_y with $\bar{x}$ are shown in Figure 19 and Figure 20. From which we can see that the change laws of C_z with $\bar{x}$ were similar at different rates and they were all negative, implying the side force acting on the UUV-1 was suction; the larger the relative velocity was, the smaller the absolute value of C_z was corresponding to the same C_z, but the difference between which was small, in other words, improvement of the local Reynolds number of the UUV-1 can decrease the interference of the submarine on its side force coefficient slightly; the influence of different velocities on M_y was the same as C_z, i.e. improvement of the local Reynolds number of the UUV-1 can also decrease the interference of the submarine on its side force coefficient modestly.

3.2 Simulation research on the motion of the UUV vertical to the submarine's longitudinal axis

We also elected the light body UUV-1 and SUB-1 as the research objects and the simulation time step was 0.2s. Considering the condition that the UUV-1 approached the submarine vertical to the its longitudinal axis from three initial positions side1-8m, side2-8m and side3-8m, the change rules of the hydrodynamic coefficients of the UUV-1 with $\bar{x}$ were investigated. The specific calculation results are shown in Figure 21 to Figure 24.

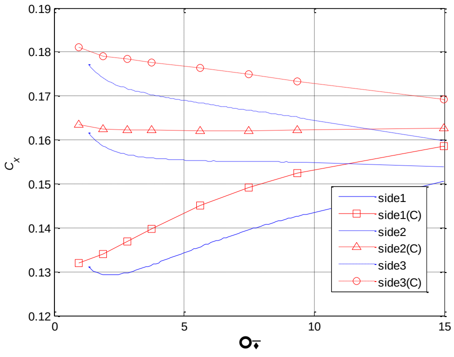

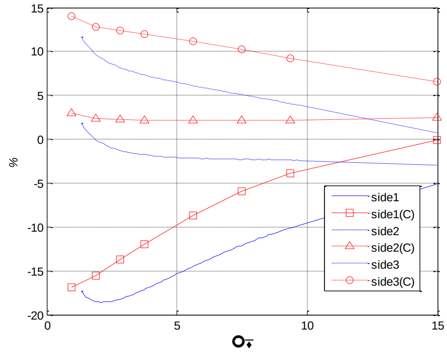

Figure 21 Calculated results of C_x **Figure 22 The change percentage of C_x**

The simulation results of C_x and its change percentage corresponding to $\Delta\bar{s}$ are as shown in Figure 21 and Figure 22. It can be seen that with the UUV-1 approaching SUB-1 laterally, when SUB-1 was located in the side1 feature orientation, $\Delta\bar{s}$ >2.8, C_x showed approximate linear decrease, when $\Delta\bar{s}$ <2.8 it displayed approximate parabolic increase; in side 2 feature orientation, when $\Delta\bar{s}$ >2.8, C_x increased slowly with the decrease of $\Delta\bar{s}$, but once $\Delta\bar{s}$ <2.8, it increased significantly; in side3 feature orientation, when $\Delta\bar{s}$ >2.8, with the decrease of $\Delta\bar{s}$, C_x showed an approximate parabolic increase trend, while $\Delta\bar{s}$ >2.8, it turned out approximate parabolic increase. Compared steady with unsteady numerical results in Figure 22, we can discover that when $\Delta\bar{s}$ >2.8, changes of the two results were similar to each other, and the calculated value in unsteady state was smaller than that in steady state corresponding to the same $\Delta\bar{s}$; when $\Delta\bar{s}$ <2.8, the change gradient of C_x with $\Delta\bar{s}$ was larger in unsteady state.

The simulation results of C_z and M_y corresponding to $\Delta\bar{s}$ when the UUV-1 approaching the SUB-1 from different positions are as shown in Figure 23 and Figure 24. From the graphic results it can be seen that with the UUV-1 getting close to the SUB-1, due to the interference of the submarine, C_z was positive , manifested as repulsion; M_y was also positive, presented as deviating the head of the UUV-1 from the SUB-1.

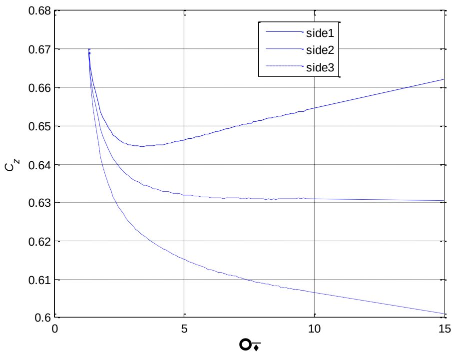

Figure 23 C_z

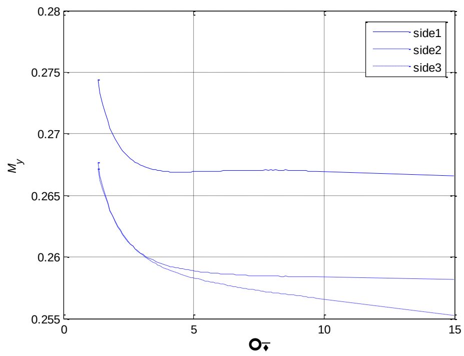

Figure 24 M_y

Conclusions

In this paper RNG $k-\varepsilon$ turbulence model was used to close the RANS equations, and combined with the dynamic grid techniques, unsteady and steady hydrodynamic performance was numerically calculated when the UUV was recovered by the submarine.

When the UUV maintained static relative to the submarine and the distance $\Delta\bar{s}$ between them is small, the hydrodynamic interference of the submarine on the UUV is strong, and with the increase of $\Delta\bar{s}$, it weakens, and the function distance of the flow around the submarine on C_x is about 30 times its diameter; the more rear the longitudinal position is, the larger C_x is. The UUV will also be subjected to the suction of the submarine for the flow around the submarine. When the UUV-2 with appendages is in the same longitudinal position and the relative direction is "side" and "up", the change laws of C_x, C_{xx} and M_{xx} with $\Delta\bar{s}$ are almost identical, while in "up" position, it is more complicated as a result of the wake flow of the fairwater. In the same feature position, for the UUV-1 and UUV-2, the change rules of C_x, C_z and M_y with $\Delta\bar{s}$ are similar accordingly.

When the UUV moves paralleled to the submarine's longitudinal axis at various speeds, the larger the local Re is, the smaller resistance coefficient is; even though the UUV is also subjected to the suction and yawing moment, the velocity has little effect on them. When the UUV approaches the submarine laterally in different feature positions, the change rules of the resistance coefficient of the UUV is similar to that in steady state; C_z is positive , manifested as repulsion; M_y is also positive, presented as deviating the head of the UUV from the submarine.

References

[1] Nicholson JW, Healey AJ.(2008) The Present State of Autonomous Underwater Vehicle (AUV) Applications and Technologies, *Marine Technology Society Journal* **42**, 44-51.

[2] Yeung, R W，Hwang, W. (1977) Nearfield hydrodynamic interactions of ships in shallow water, *Journal of Hydronautics* **11**, 128-135.

[3] H. Zhang, W.H. Melbourne. (1992) Interference between two circular cylinders in tandem in turbulent flow, *Journal of Wind Engineering and Industrial Aerodynamics* **41**, 589-600.

[4] Zeng YF, Zhu JM. (1994) Discussion on the calculation of the hydrodynamic interaction between underwater moving objects, *The Ocean Engineering* **02**, 40-48.

[5] Y.R. Choi, S.Y. Hong. (2002) An analysis of hydrodynamic interaction of floating Multi-Body Using Higher-Order Boundary Element Method, *The Twelfth International Offshore and Polar Engineering Conference*, Kitakyushu, Japan.

[6] Wang F. (2003) Hydrodynamic calculation on an autonomous underwater vehicle in motion near a submarine , Harbin Engineering University.

[7] B.J. Koo, M.H. Kim, (2005) Hydrodynamic interactions and relative motions of two floating platforms with mooring lines in side-by-side offloading operation, *Applied Ocean Research* **27**, 292-310.

[8] S.Y. Hong, J.H. Kim, S.K. Cho, Y.R. Choi, Y.S. Kim. (2005) Numerical and experimental study on hydrodynamic interaction of side-by-side moored multiple vessels, *Ocean Engineering* **32**, 783-801.

[9] Cheng L, Zhang Liang, Wu Deming, Chen Qiang. (2005) Hydrodynamic interactions between two underwater non- lifting bodies, *Journal of Harbin Engineering University* **26**, 1-6.

[10] Zhang L, Cheng L, et al. (2006) Experiment on Hydrodynamic Interaction Between 2D Oval and Wall, *Journal of Ship Mechanics* **10**, 1-10.

[11] Cheng L. (2006) Research on hydrodynamic interactions between two bodies, Harbin Engineering University.

[12] He YZ. (2010) Study on the control of UUV with cable during recovery, Northwestern Polytechnical University.

[13] Leong Z, Saad K, et al. (2013) Investigation into the hydrodynamic interaction effects on an AUV operating close to a submarine, Pacific international maritime conference, 1-11.

[14] S.A.T. Randeni P., Z.Q. Leong, D. Ranmuthugala, A.L. Forrest, J. Duffy. (2015) Numerical investigation of the hydrodynamic interaction between two underwater bodies in relative motion, *Applied Ocean Research* **51**, 14-24.